TU Delft

Delft University of Technology

Document Version
Final published version

Licence
Dutch Copyright Act (Article 25fa)

Citation (APA)
Zhang, W., Zou, J., Wei, Z., Han, Z., Yang, L., & Zhang, W. (2026). Modifying stacking sequences to leverage the effects of shear thickening gel (STG) on the impact resistance of the STG applied carbon fibre-reinforced polymer (SACFRP) composite laminates. *Composites Science and Technology*, *273*, Article 111414. https://doi.org/10.1016/j.compscitech.2025.111414

Important note
To cite this publication, please use the final published version (if applicable).
Please check the document version above.

Copyright
In case the licence states “Dutch Copyright Act (Article 25fa)”, this publication was made available Green Open Access via the TU Delft Institutional Repository pursuant to Dutch Copyright Act (Article 25fa, the Taverne amendment). This provision does not affect copyright ownership.
Unless copyright is transferred by contract or statute, it remains with the copyright holder.

Sharing and reuse
Other than for strictly personal use, it is not permitted to download, forward or distribute the text or part of it, without the consent of the author(s) and/or copyright holder(s), unless the work is under an open content license such as Creative Commons.

Takedown policy
Please contact us and provide details if you believe this document breaches copyrights.
We will remove access to the work immediately and investigate your claim.

This work is downloaded from Delft University of Technology.

Composites Science and Technology 273 (2026) 111414

Contents lists available at ScienceDirect

Composites Science and Technology

journal homepage: www.elsevier.com/locate/compscitech

Modifying stacking sequences to leverage the effects of shear thickening gel (STG) on the impact resistance of the STG applied carbon fibre-reinforced polymer (SACFRP) composite laminates

Wanrui Zhang [a,1], Jianchao Zou [a,1], Zongyou Wei [b], Zhibin Han [c], Lei Yang [b], Weizhao Zhang [a,d,*]

[a] Department of Mechanical and Automation Engineering, The Chinese University of Hong Kong, Shatin, NT, Hong Kong Special Administrative Region
[b] Department of Civil Engineering, College of Civil and Transportation Engineering, Shenzhen University, Shenzhen, 518060, China
[c] Faculty of Aerospace Engineering, Delft University of Technology, Kluyverweg 1, 2629 HS, Delft, the Netherlands
[d] Institute of Intelligent Design and Manufacturing, The Chinese University of Hong Kong, Shatin, NT, Hong Kong Special Administrative Region

ARTICLE INFO

Keywords:
Shear thickening gel (STG)
STG applied carbon fibre-reinforced polymer (SACFRP)
Low-velocity impact (LVI)
Interfacial toughening
Stacking sequences

ABSTRACT

In this work, shear-thickening-gel applied CFRP (SACFRP) composite laminates were developed to enhance the impact resistance of the composites under low-velocity impact (LVI) conditions, where the incorporated shear thickening gel (STG) worked as the interphase material between fibres and resin matrix. To analyse the effects of STG in its composites, static tensile and shear tests were first conducted on longitudinally and transversely positioned unidirectional (UD) SACFRP and its CFRP reference, respectively. Experimental results indicated that the corresponding reduction of the resin matrix due to the incorporation of the relatively soft STG weakened the interlaminar behaviour of the SACFRP laminates during static mechanical tests. However, the transverse tensile toughness of the SACFRP exhibited a remarkable 139 % improvement compared to the CFRP reference, demonstrating significant interfacial toughening of the developed composites, as verified through SEM analysis. To leverage the effects of the STG on the composites, this work modified the stacking sequences of SACFRP laminates. LVI tests and recurring LVI tests demonstrated the substantial improvement of impact performance for layup-designed SACFRP laminates since the impact-resistant mechanism transitioned from the local damage of CFRPs to the global flexural behaviour of SACFRPs. Timoshenko's analytical model validated the resistant mechanism transition of layup-designed SACFRP during LVI tests. Therefore, the SACFRP laminates with modified stacking sequences demonstrate outstanding potential for use under extreme loading conditions involving complex and unavoidable impacts, highlighting their broad applicability across various industries.

1. Introduction

Owing to the high performance-to-weight ratios and superior properties, CFRP composites demonstrate significant prospects for extensive applications in multiple industrial fields, including aviation, automotive, and energy [1–3]. Notably, the global carbon fibre-reinforced polymers (CFRPs) market has experienced sustained expansion over the last two decades with a compound annual growth rate of approximately 12.5 % [4]. However, brittle behaviour dominates the failure process of the carbon fibre reinforcement [5], and the polymer matrix tends to embrittle under dynamic loading conditions [6]. The inherent brittleness renders composite structures made of CFRPs susceptible to low-velocity impact (LVI) throughout manufacturing, service, and maintenance, which limits their broader utilisation [7]. For instance, LVI is one common type of load in aeronautics, from debris impacts to maintenance tool drops [8].

Commonly employed methods to improve the LVI performance of CFRPs involve modifying the component materials or developing hybrid structures. Particularly, numerous investigations have focused on adapting the resin matrix of CFRPs to reduce the brittleness and enhance

* Corresponding author. Department of Mechanical and Automation Engineering, The Chinese University of Hong Kong, Shatin, NT, Hong Kong Special Administrative Region.
E-mail address: weizhaozhang@cuhk.edu.hk (W. Zhang).
[1] Wanrui Zhang and Jianchao Zou contributed equally to this manuscript.

https://doi.org/10.1016/j.compscitech.2025.111414
Received 19 May 2025; Received in revised form 31 August 2025; Accepted 10 October 2025
Available online 10 October 2025
0266-3538/© 2025 Elsevier Ltd. All rights are reserved, including those for text and data mining, AI training, and similar technologies.

the impact-resistant performance of these composites. For instance, a 53 % increase in structural integrity was noted for thermoplastic CFRP laminates during LVI tests compared to their thermoset counterparts [9]. Recent work incorporated thermoplastic ε-caprolactone into the thermoset resin matrix of CFRPs and found that it substantially improved their self-healing capability and impact performance [10]. Moreover, core-shell rubber nanoparticles and modifications to the block copolymer matrix have been utilised to augment the interlaminar fracture toughness of the CFRPs by 45 %, leading to a significant enhancement in their damage resistance during impact events [11]. Besides adapting the resin matrix, modifying fibre reinforcement provides CFRP composites with higher strength, toughness, and energy absorption, thus strengthening the impact-resistant performance [12]. For example, introducing glass fibres into CFRP laminates can remarkably improve their impact resistance and post-impact mechanical performance [12,13]. Integrating silk and carbon fibres can also enhance the LVI performance of epoxy-based composites, providing a 123 % increase in impact strength compared to the pure CFRP reference [14]. However, the increased complexity and cost might hinder these modified designs of component materials from large-scale utilisation.

On the other hand, hybrid structures, such as hybrid fibre-metal laminates, have been developed over decades, addressing the inadequate impact resistance of CFRPs [15]. For instance, the stainless-steel wire mesh/CFRP composites manufactured through the vacuum-assisted resin infusion (VARI) technique exhibit significantly reduced internal damage during impacts [16]. This improvement arises from the ductility of the steel wire mesh that can dissipate the energy throughout the cross-section and allows the structure to absorb more energy than CFRP references [16]. Besides, hybrid titanium composite laminates can provide superior impact-resistant benefits relative to traditional fibre-reinforced polymer (FRP), particularly in applications under challenging environmental conditions [17]. While the impact resistance of hybrid composites substantially improves, this approach unavoidably increases the density and thickness of the CFRPs, undermining their inherent lightweight benefit. Therefore, it seems to be more promising to incorporate the lightweight and effective materials into CFRPs for their impact-resistant enhancement.

Recent years have witnessed considerable efforts for the development of shear-thickening materials (STMs) and their associated composites, as STMs can provide impressive impact resistance. The visible mechanoluminescence technique was employed to illustrate the impact-resistant mechanism of the shear thickening gel (STG) [18]. It was found that the shear thickening behaviour and viscoelastic deformation of the STG contribute to the enlargement of the impact area and the enhanced energy absorption properties under impact loads [18]. Therefore, multiple works have developed composites integrated with STMs to resist impact loads. For instance, a fourfold increase in energy absorption was found for tube structures made of silicone gel composites filled with shear-thickening fluid (STF) during dynamic loads [19]. A gradient-stacked STF/Kevlar fabric multi-layer armour has also been developed with remarkable impact attenuation while preserving its lightweight characteristics [20]. Furthermore, a notable improvement in the ballistic performance of STF-impregnated Kevlar fabric was recorded, too, with the enhancement linked to strengthening and energy absorption properties of the STF, as confirmed through a comprehensive experimental and modelling methodology [21]. Prior studies primarily incorporate STMs into flexible composites, and limited research concentrates on developing STM-based structural composites. However, plenty of applications, such as helmets, shields, carbon plates, sports protective equipment, and EV battery enclosures, demand lightweight rigid materials with not only load-bearing but also impact-resistant capabilities. Therefore, this study aims to enhance the impact-resistant performance of CFRPs by integrating STG into composites as the interphase material between the fibre reinforcement and polymer matrix. In addition, since the STG has a lower density than the polymer matrix, the developed STG-applied CFRP (SACFRP) is more lightweight than the hybrid fibre-metal composites.

In this work, static tensile and shear tests were conducted on the longitudinally and transversely positioned unidirectional (UD) SACFRP specimens to investigate the effects of the STG on the composites. The substantial increase in transverse tensile toughness of the SACFRPs revealed interfacial toughening effects of the STG on its composites. Furthermore, this work modified the stacking sequence of the SACFRP laminates to leverage these effects. Specifically, SACFRPs with proper lay-up design possess static properties comparable to those of the CFRP and also demonstrate greatly reduced integrity loss and significantly increased accumulated energy absorption during LVI and recurring LVI (RLVI) tests.

2. Materials and methods

2.1. Component materials of the composites

This study selected the commercial thermoset epoxy polymer, Epolam 5015, as the resin matrix for composite laminates since Epolam is among the most widely utilised epoxy resins in engineering applications [22]. Axson Technologies supplied the Epolam 5015 resin and associated amine hardener used in this work. The formulation of Epolam polymer requires the uniform mixture of its resin and hardener in the mass ratio of 10:3, as specified in the material datasheet [23]. After the impregnation into carbon fabrics, the Epolam polymer was cured at 80 °C for 8 h to achieve optimal mechanical and thermal properties [24].

Polymer Technologies PTE LTD provided the L300-C UD carbon fabrics used in this work. These fabrics were cut into squares with a side length of 250 mm and subsequently subjected to ultrasonic cleaning to remove the residual dust particles. Before the fabrication of composite laminates, the fabrics were oven-dried and subsequently stored in a dry cabinet maintained at room temperature and 25 % relative humidity. Table 1 lists the material properties of the UD carbon fabric, as provided by the supplier.

Boric acid and hydroxyl silicone oil are the primary raw materials used in this work for the synthesis of STG. This work also introduced oleic acid at a mass fraction of 1 wt% to enhance the plasticity of STG and facilitate vulcanisation. These raw materials were blended in the kneader vessel under specified pressure and thermal settings, initiating the polymerisation process and the formation of STG. Detailed preparation information can be found in reference [25].

2.2. Fabrication process of the SACFRP composites

Fig. 1 demonstrates the fabrication process of the SACFRP laminates. At first, the STG was dissolved in xylene with the solute and solvent in the mass ratio of 1:5. Afterwards, the uniformly blended solution was dipped into the fabrics to prepare the flexible STG-applied carbon fabrics (SACF). Careful scraping is required to ensure the solution can completely impregnate the carbon fibres. After evaporation of the xylene solvent, the solidified SACFRP laminates were fabricated by utilising the prepared flexible SACF and Epolam polymer, and through the hot-press moulding technique at the temperature of 80 °C and the loading pressure of 50 kPa for 8 h. Given that the epoxy matrix was introduced to fabricate the cured laminates after the preparation of SACF, the STG worked as the interphase material between carbon fibres (CFs) and the epoxy matrix. The manufacturing process of the reference CFRP laminates was identical to that of the SACFRP laminates. The

Table 1
Fibre properties of the UD carbon fibre fabric L300-C used in this work.

Tensile modulus (GPa)	Tensile strength (MPa)	Elongation at break (%)	Fibre filaments (tex)	Fibre coating/ size
230	4900	2.1	800	Epoxy

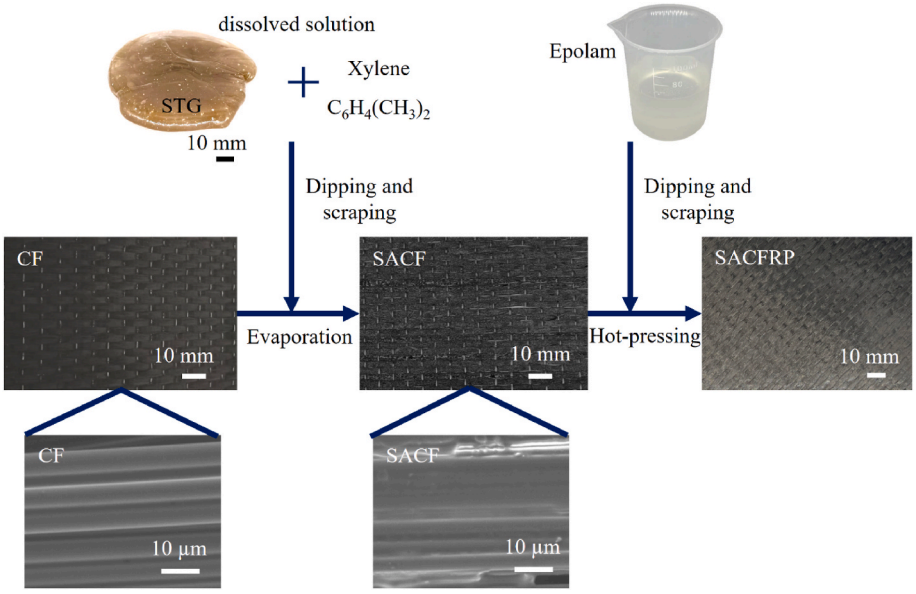

Fig. 1. Fabrication process of the SACFRP laminates.

water jetting technique was used to cut the fabricated laminates into the tensile, shear, and LVI specimens based on ASTM D3039 [26], ASTM D5379 [27], and ASTM D7136 [28], respectively.

Fig. 1 also illustrates SEM results of the SACF and its carbon fabric (CF) reference. In contrast to bare fibres of the CF reference, SACF has carbon fibres entirely enveloped by the STG, indicating the tight bonding between STG and carbon fibres within SACF.

The volume fraction of the component materials in the final composite laminates was determined based on the density and mass measurements. Specifically, this work quantified the mass of the pre-fabrication fabrics and post-fabrication laminates using an electronic scale with an accuracy of 0.1 g. Besides, the buoyancy method was used to measure the density of the cured Epolam, carbon fabrics, STG, and composite laminates using a digital electronic analytical balance scale with an accuracy of 0.01 mg [29]. Table 2 presents the density and volume fraction of all the materials utilised in this work. Notably, the STG has a density of 0.91 g/cm^3, which is lower than the density of 1.09 g/cm^3 of the Epolam polymer. Particularly, the SACFRP composite laminates exhibit a density of 1.38 g/cm^3, which is 4.7 % lower than that of the CFRP reference. Hence, the developed SACFRP demonstrates the lightweight advantage in engineering applications compared with the hybrid fibre-metal composites with the average density of 3.56 g/cm^3 [17]. Table 2 lists the volume fraction values of the component materials in the SACFRP laminates and the CFRP counterparts. It is worth mentioning that all laminates used in this work were controlled to maintain a similar volume fraction of fibres at approximately 59.3 %, as listed in Table 2.

Table 2
Density and volume fraction of the materials in this work.

Materials	Density (g/cm^3)	Volume fraction in the CFRP (%)	Volume fraction in the SACFRP (%)
CFRP	1.46	100.0	NA
SACFRP	1.38	NA	100.0
STG	0.91	NA	25.8
Epolam resin	1.09	40.6	15.0
Carbon fabrics	1.65	59.4	59.2

2.3. Static mechanical tests

Static tensile and shear tests were performed on the composite specimens according to the standards of ASTM D3039 [26] and ASTM D5379 [27]. Fig. 2 demonstrates the static mechanical test setup employed in this work. Specifically, the test setup consisted of a universal testing machine (UTM) and a digital image correlation (DIC) system. The hydraulic-powered UTM used in this study features adjustable clamps, allowing for the implementation of different fixtures for the planned mechanical tests. The DIC system was employed to conduct strain analysis by capturing the displacement and deformation of the surficial speckles on the specimens. We prepared 5 specimens for each test group with the geometry following the corresponding ASTM standards, and selected at least 3 effective and representative specimens for the calculation.

2.4. LVI tests

Fig. 3 demonstrates the ASTM standard LVI test setup used in this study. The composite specimens for impact tests had dimensions of 100 mm in width, 150 mm in length, and an average thickness of 2.4 mm. These samples were placed between rubber-tipped fixtures, providing a rectangular impact area measuring 75 mm in width and 125 mm in length. The impactor, weighing 6.27 kg, is equipped with a hemispherical striker with a diameter of 12.7 mm. This impactor falls along two smooth guiding columns from the height corresponding to the specified impact energy, and it incorporates a data collection system to record impact load and contact time during LVI tests. The velocity and displacement are calculated using the ASTM D7136 standard [28]. High-speed cameras capturing images at 80,000 frames per second were utilised to capture the bottom surface of the samples for fracture mechanism analysis. Furthermore, two hydrargyrum medium-arc iodide (HMI) lamps were positioned beneath the fixture to illuminate the bottom surface of the specimens.

Fig. 4 (a) and (b) illustrate typical force-displacement and energy-time curves, respectively, for the CFRP laminates during LVI tests. Particularly, the force-displacement curve provides insights into the peak force (F_p), the displacement at peak force (PD_m) and the maximum displacement (PD_u) of the specimens during LVI tests, as demonstrated in Fig. 4 (a). Based on these basic impact characteristics, the stiffness (F_p/PD_m) and the integrity loss (PD_u-PD_m) can be correspondingly

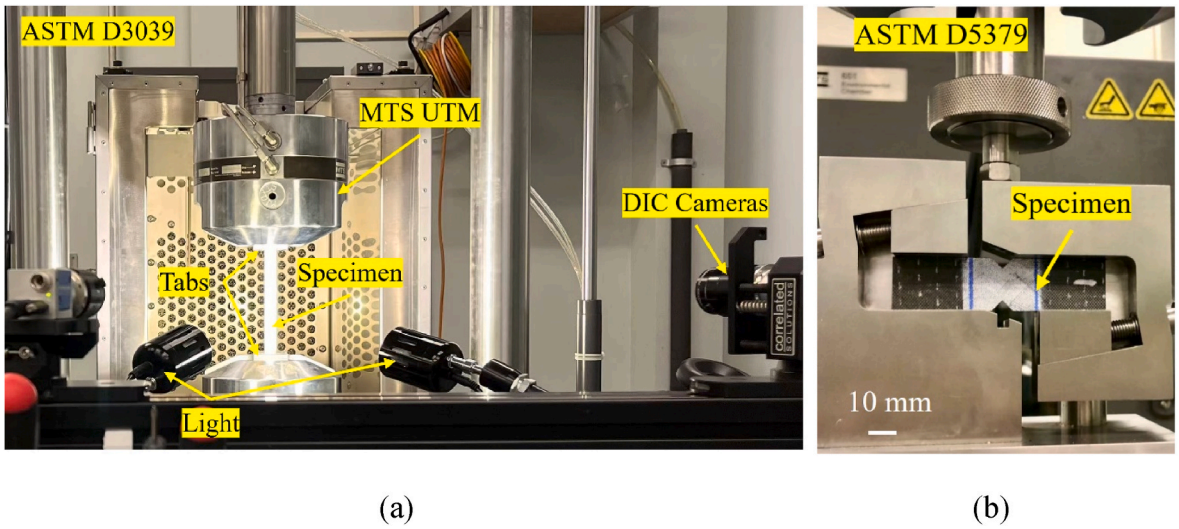

Fig. 2. Experimental setup of the (a) tensile and (b) shear tests.

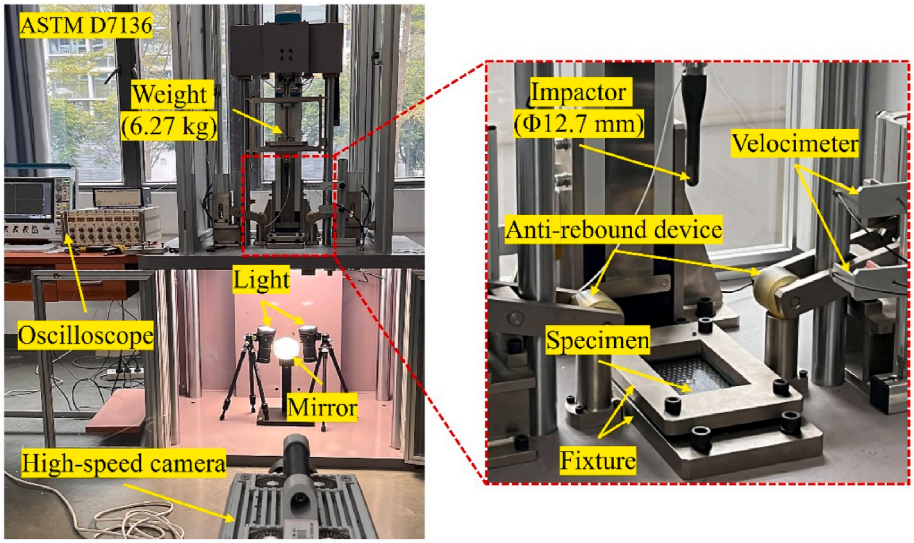

Fig. 3. Experimental setup of the LVI tests.

calculated [9]. The energy-time curve in Fig. 4 (b) provides information about the finally absorbed energy (E_a), the elastic energy (E_e) and the impact energy ($E_a + E_e$).

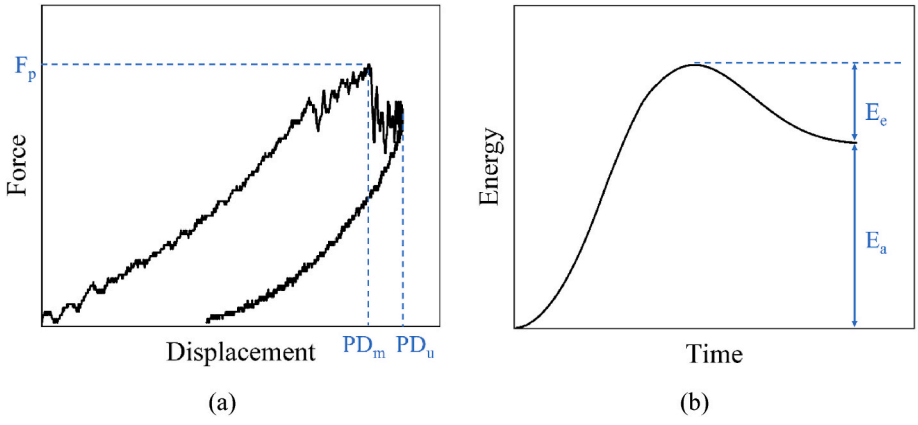

Fig. 4. Typical (a) force-displacement, and (b) energy-time curves of the CFRP laminates during LVI tests.

3. Results and discussion

3.1. Properties of STG in this work

The storage modulus characterises the ability of a material to store elastic deformation energy in its solid-like state, while the loss modulus reflects its viscosity in the liquid-like state [20]. In this work, the frequency sweep tests were conducted for the prepared STG using the rheometer to assess its shear thickening behaviour. Fig. 5 (a) illustrates the storage and loss modulus of the STG in this work as the frequency increases from 0.1 Hz to 100.0 Hz. The storage modulus of the STG increases by over two orders of magnitude to 250.34 kPa at 100.0 Hz from 1.53 kPa at 0.1 Hz, demonstrating its significant shear thickening behaviour [30]. The loss modulus of the STG rises from 8.44 kPa at 0.1 Hz to the peak value of 84.24 kPa at 4.0 Hz before decreasing to 33.33 kPa at 100.0 Hz. The intersection of the storage and loss modulus curves indicates the phase transition of the STG, shifting from the liquid-like to the solid-like state at the critical frequency of approximately 3.5 Hz.

For a clearer demonstration, the STG with the mass of approximately 3 g cannot lift a 1 kg weight under slow pulling conditions, but it can when subjected to rapid pulling, as illustrated in Fig. 5 (b). Inspired by the enhanced dynamic mechanical behaviour of the STG, this work aims to harness the shear thickening performance of STG to improve the impact resistance of the CFRPs under LVI conditions.

Fig. 6(a) and (b) (a) and (b) illustrate the effects of temperature on storage and loss moduli, respectively, for the STG under the shear frequency of 0.01 Hz, 1 Hz, and 100 Hz. Specifically, a minimal decrease is found for moduli of the STG at low shear frequency with the increment of temperature, while both moduli at high shear frequency remain constant under various thermal conditions. Therefore, shear thickening of the STG increases slightly as temperature rises from room temperature to 80 °C, implying environmental stability of it and its composites.

3.2. Effects of STG on static mechanical behaviour of the UD SACFRP

During the longitudinal tensile process, when failure of the UD CFRP specimens occurred, the clicking sound occurred first, corresponding to the initial matrix crack [31]. Afterwards, the intensity of this sound escalated with the increasing load due to the increasingly severe localised stress concentration. Finally, the explosive sound was noted at the rupture of specimens. For the UD SACFRP, on the other hand, there is no progressive clicking sound before the sudden load drop during the longitudinal tensile tests.

Fig. 7 depicts the representative stress-strain responses of the SACFRP and its CFRP reference during the longitudinal tensile tests. The representative specimen was selected among 5 samples to be the one with strength closest to the average strength of the testing group. Test results demonstrate the equivalent longitudinal tensile modulus between the CFRP and SACFRP, which is reasonable since they have similar volume fractions of the dominant fibres [32]. In contrast, the longitudinal tensile strength of the UD SACFRP decreased by around 33.3 % compared to its CFRP reference. The following failure analysis elucidates the mechanism underlying the longitudinal tensile strength decrease of the UD SACFRPs.

Fig. 8 demonstrates failure modes of the UD CFRP and SACFRP specimens after the longitudinal tensile tests. As shown in Fig. 8, the longitudinal splitting damages are dispersedly distributed in the CFRP specimens, coinciding with the progressive damage process of the UD CFRP during the tests. Notably, the progressive damage in the UD CFRPs during the tests indicates that new damage sites can emerge as the load increases, resulting in scattered fracture patterns throughout specimens [33]. In contrast, fewer fracture characteristics within the gauge range of each SACFRP specimen indicate the instantaneous failure of SACFRP upon the initial matrix crack, which corresponds to the absence of continuous clicking sounds before complete failure of the SACFRP specimens during tests. Hence, the failure analysis verifies that the SACFRP cannot withstand the longitudinal tensile load immediately following the initial matrix crack. The longitudinal tensile strength reduction of UD SACFRP can be attributed to the low volume fraction of the solidified Epolam matrix and the gel state of the STG under static loading, as demonstrated in Table 2 and Fig. 5 (b), respectively. Specifically, the decreased fraction of solidified epoxy matrix in the SACFRP reduced its stress transfer capacity to withstand the initial matrix cracking.

Fig. 9 (a) illustrates the shear stress-strain behaviour of the longitudinally positioned SACFRP and its CFRP reference during static shear tests. The initial longitudinal shear modulus of the SACFRP closely resembles that of its CFRP reference due to the same fibre volume fraction. Fig. 9 (b) demonstrates the failure modes of the UD SACFRP and CFRP after longitudinal shear tests. Particularly, the delamination failure can be observed from the side view of both the SACFRP and CFRP, which dominates the fracture process of the UD composite specimens during longitudinal shear tests [34,35]. Consequently, the interlaminar performance of the SACFRP and CFRP can be revealed through the longitudinal shear tests. It could be inferred from the reduction of shear strength in Fig. 9 (a) that incorporation of the STG into the composite laminates significantly diminished the interlaminar strength when subjected to static loads. Matrix cracking is the primary cause of delamination in composite laminates [36]. Therefore, the reduced matrix in the SACFRP leads to earlier delamination than that of the CFRP reference, limiting the longitudinal shear strength of SACFRPs.

Table 3 lists longitudinal tensile (LT) and longitudinal shear (LS) strength and moduli of the UD CFRP and SACFRP.

Fig. 10(a) and (b) demonstrate the stress-strain curves of transversely positioned UD SACFRP and CFRP during static tensile and shear tests, respectively. The reduced modulus could be attributed to the decreased

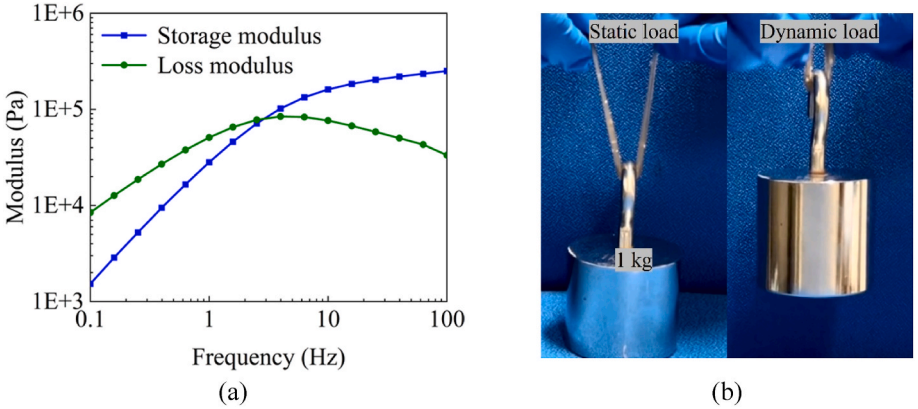

Fig. 5. (a) Storage and loss modulus curves of the STG as the shearing frequency increases, and (b) rate-dependent load-bearing behaviour of the STG.

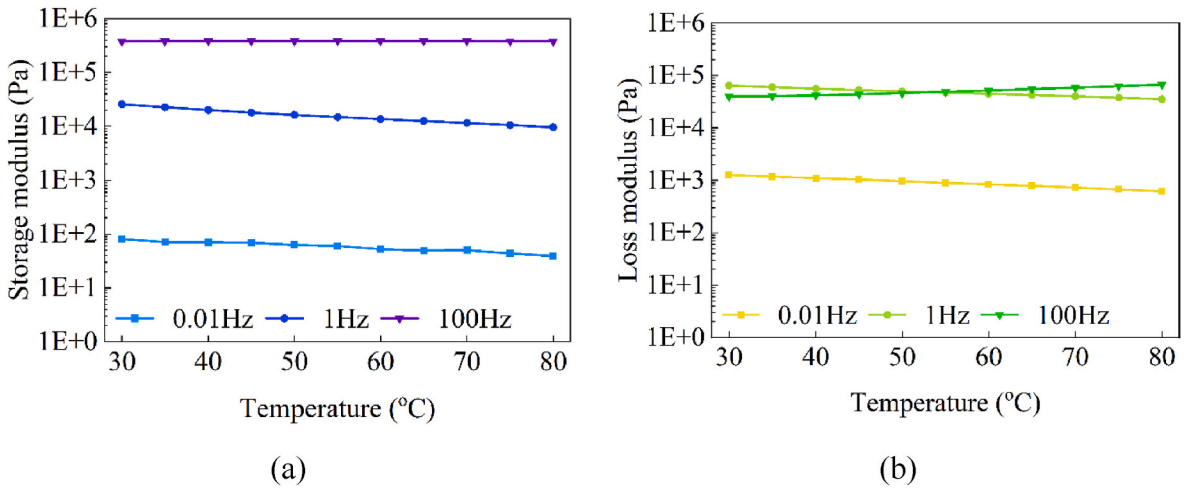

Fig. 6. Thermal effects on (a) storage, and (b) loss moduli of the STG under the shear frequency of 0.01 Hz, 1 Hz, and 100 Hz.

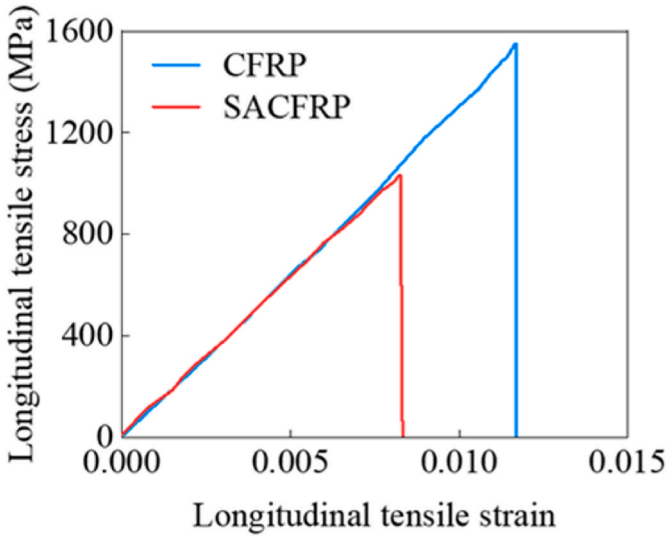

Fig. 7. Longitudinal tensile stress-strain curves of the UD CFRP and SACFRP.

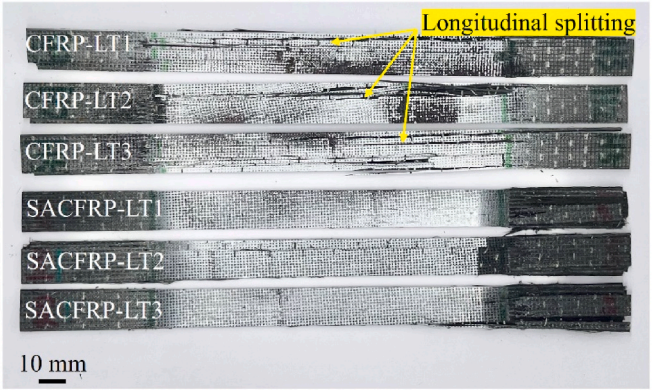

Fig. 8. Failure modes of the UD CFRP and SACFRP after longitudinal tensile tests.

volume fraction of the epoxy matrix since the cured matrix behaviour dominated the transverse modulus of CFRP [37,38]. As shown in Fig. 10 (c), UD CFRP specimens exhibit planar fracture after the transverse tensile tests, suggesting the onset of catastrophic cracks triggered by localised clusters of fibre-matrix interfacial debonding due to stress concentration [39]. In contrast, delamination and wedge-shaped fracture of SACFRP were noted in Fig. 10 (d), indicating that the interlaminar delamination and matrix cracking determine the failure modes of SACFRP [40]. Besides, it can be inferred that SACFRP exhibits significantly higher transverse toughness based on the much larger strain in Fig. 10(a) and (b). Specifically, the transverse tensile toughness of SACFRP increased by 138.95 %, indicating its highly enhanced interfacial toughness.

Furthermore, the extent of fibre-matrix interphase adhesion can be revealed based on the SEM-based fracture analysis [41]. As demonstrated in Fig. 11 (a), SEM result of the UD CFRP after transverse tensile failure illustrates the fracture surface with clean and smooth fibre surface, indicating weak interphase adhesion. In contrast, residues of Epolam matrix and STG are fairly observed on carbon fibres in the SACFRP after the transverse tensile failure, suggesting the tough interphase adhesion, as shown in Fig. 11 (b).

Table 4 lists transverse tensile (TT) and transverse shear (TS) strength and moduli of the UD CFRP and SACFRP.

3.3. LVI behaviour and failure analysis of UD SACFRP

Fig. 12 (a) and (b) depict the force-displacement curves of UD CFRP (UDC) and UD SACFRP (UDS) during LVI tests with impact energy levels of 10J, 15J, 20J, and 25J. As illustrated in Fig. 12 (a), the displacement of the UD CFRP specimens rises and then decreases, corresponding to the movement of the impactor during LVI tests. This trend is observed for the UD SACFRP specimens under LVI with impact energies below 20J, and no further decreasing displacement demonstrates the occurrence of perforation for the UD SACFRP laminates under 25J LVI. Moreover, the value of integrity loss remained minimal for the UD CFRP laminates, indicating their high structural integrity during LVI tests. In contrast, considerable integrity loss was noted for the UD SACFRP specimens during the LVI tests with impact energy exceeding 10J, suggesting severe damage to these specimens.

Fig. 13(a) and (b) illustrate the energy-time responses of the UD CFRP and UD SACFRP during LVI with various impact energy levels. The plateau-shaped energy-time curves in Fig. 13 (a) indicate no perforation in the UD CFRP. Conversely, Fig. 13 (b) demonstrates the perforation of the UD SACFRP at 25J LVI.

Longitudinal splitting can be inferred as the primary failure mode of both UD SACFRP laminates and CFRP references, as demonstrated in Fig. 14. This fracture mode revealed that the SACFRP and CFRP laminates absorbed impact energy through matrix cracking and intra-yarn splitting. Furthermore, more pronounced fractures existed in the UD

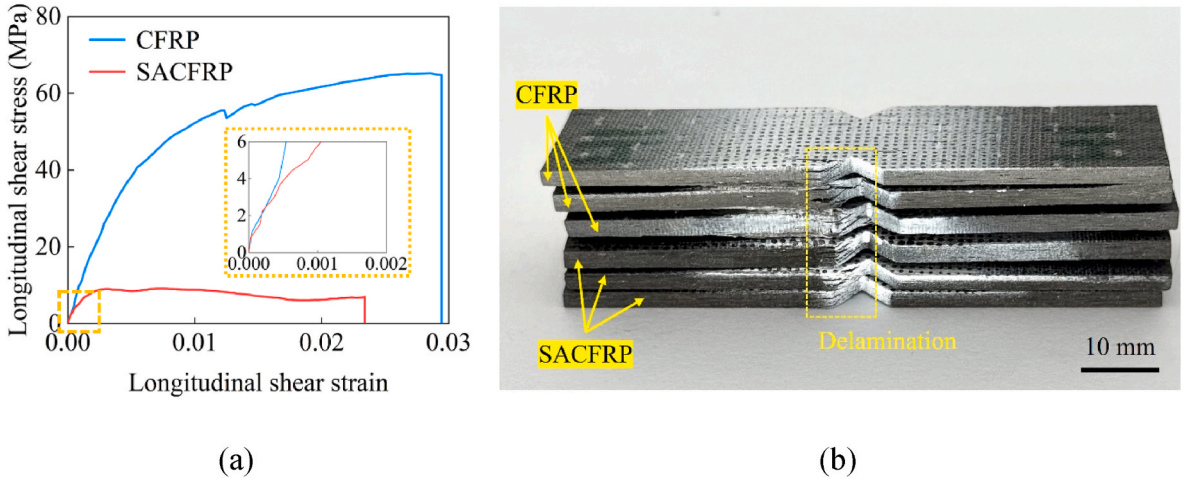

Fig. 9. (a) Shear stress-strain curves and (b) failure modes of the UD CFRP and SACFRP under longitudinal shear tests.

Table 3
Longitudinal tensile (LT) and longitudinal shear (LS) strength and modulus of the UD CFRP and SACFRP.

Properties	CFRP-LT	SACFRP-LT	CFRP-LS	SACFRP-LS
Strength (MPa)	1532.81 ± 38.25	987.98 ± 81.70	67.15 ± 1.77	15.33 ± 2.98
Modulus (GPa)	129.87 ± 3.73	127.35 ± 4.14	11.00 ± 0.17	7.67 ± 1.67

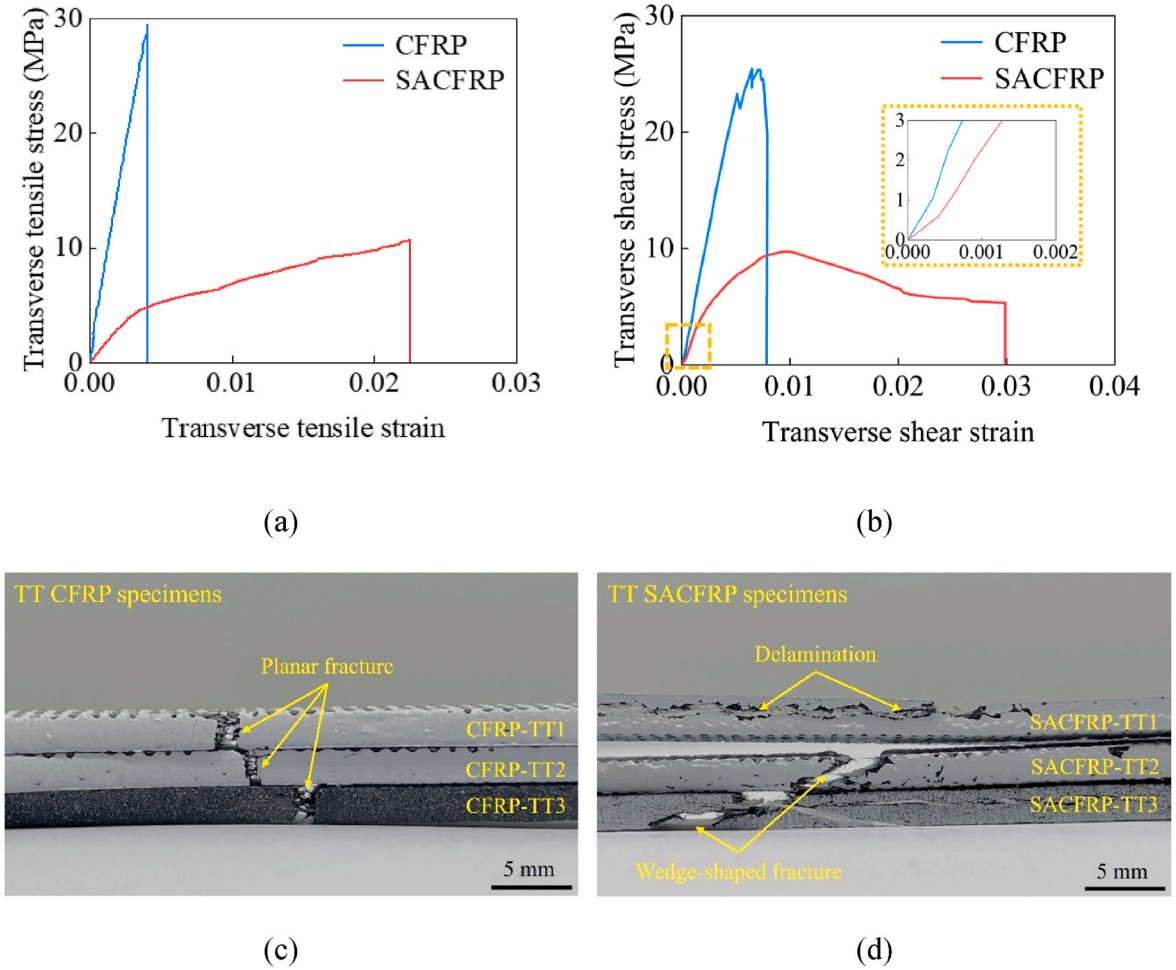

Fig. 10. (a) Transverse tensile, and (b) transverse shear stress-strain curves of the UD CFRP and SACFRP. Failure modes of the (c) UD CFRP and (d) UD SACFRP under transverse tension.

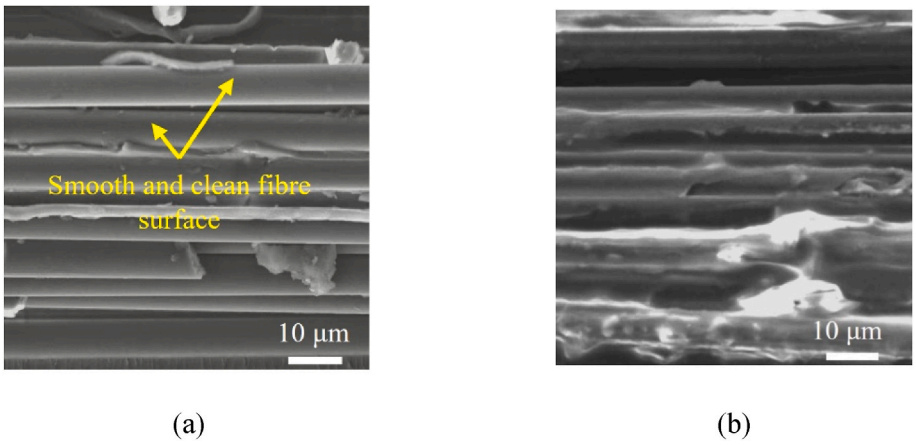

Fig. 11. SEM-based fracture analysis of the (a) UD CFRP and (b) UD SACFRP after transverse tensile tests.

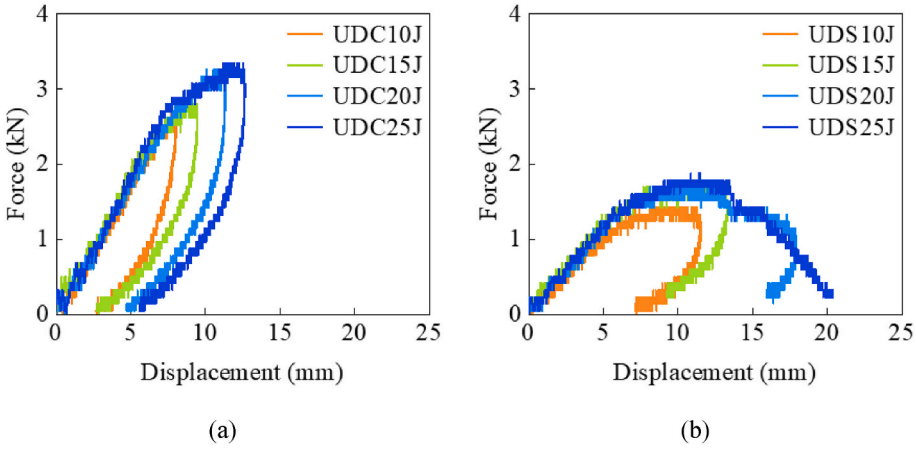

Fig. 12. Force-displacement responses of the (a) UDC and (b) UDS specimens under LVI with different impact energies.

Table 4
Transverse tensile (TT) and transverse shear (TS) strength and modulus of the UD CFRP and SACFRP.

Properties	CFRP-TT	SACFRP-TT	CFRP-TS	SACFRP-TS
Strength (MPa)	28.15 ± 1.01	11.17 ± 0.02	28.27 ± 1.27	13.15 ± 2.04
Modulus (GPa)	7.34 ± 0.51	1.42 ± 0.02	5.44 ± 0.42	2.37 ± 0.40

SACFRP specimens during LVI tests, indicating that the low volume fraction of the matrix in this composite leads to its low impact-resistant performance.

3.4. Static mechanical performance of layup-designed SACFRPs

Fig. 15 (a) illustrates the stress-strain curves of the SACFRP and its CFRP reference with the stacking sequence of $[45/90/135/0]_s$ during static tensile tests. Compared to the longitudinal and transverse tensile

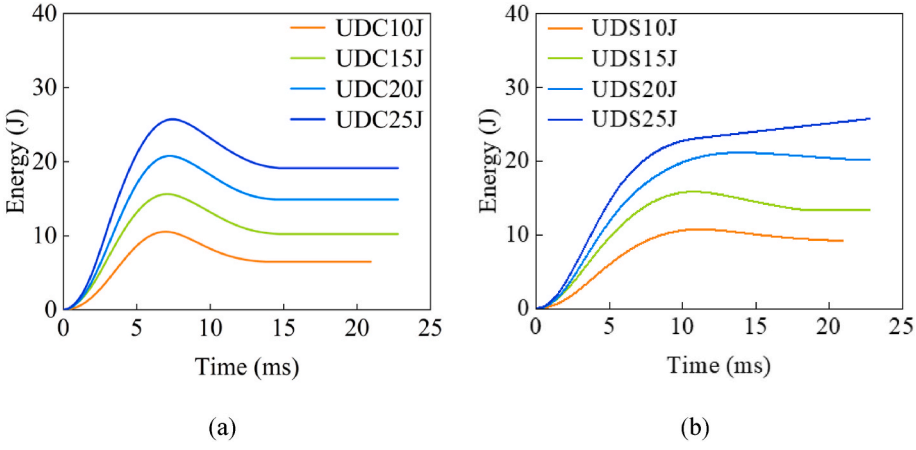

Fig. 13. Energy-time responses of the (a) UDC and (b) UDS specimens under LVI with different impact energies.

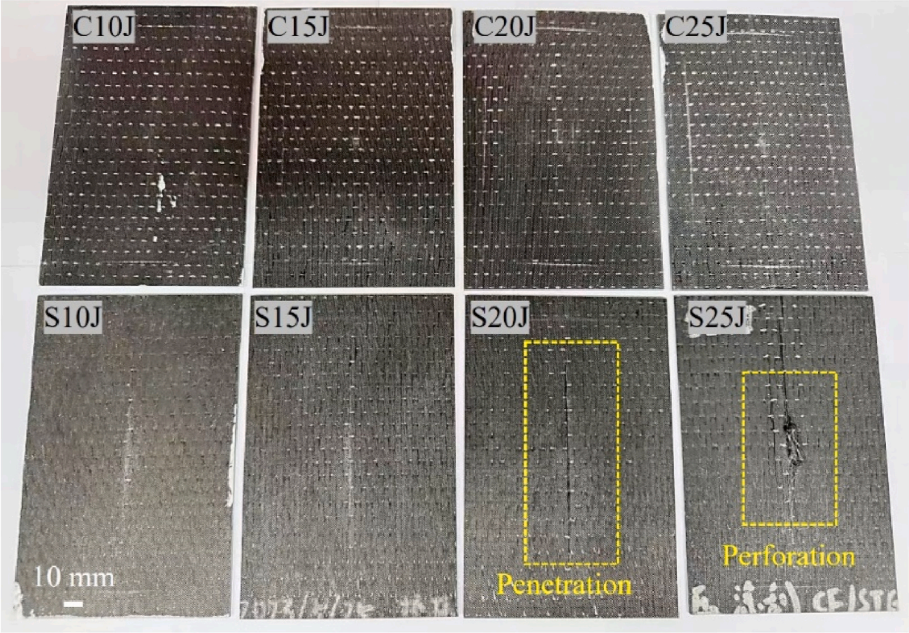

Fig. 14. UD CFRP and UD SACFRP specimens after LVI tests.

responses of the UD SACFRP, the tensile behaviour of the lay-up designed SACFRP demonstrates mechanical properties more closely aligned with its CFRP reference. As shown in Fig. 15 (b), the retentions of specific tensile toughness, modulus and strength are 88.8 %, 93.7 % and 84.2 %, respectively, for the layup-designed SACFRP laminates compared to the CFRP references.

The static mechanical performance of the layup-designed SACFRP is comparable to that of the CFRP reference, suggesting that proper layup design of the SACFRP can effectively alleviate the influence of reduced epoxy matrix. In the UD CFRP and SACFRP laminates, the Epolam matrix primarily transfers stress between fibres. Therefore, the reduced volume fraction of the polymer matrix limits stress transfer of the UD SACFRP laminates, resulting in their drastically reduced static mechanical strength. In the lay-up designed CFRP and SACFRP, fibres are oriented along multiple directions, allowing all different loads to be mainly borne by the fibres. As a result, the layup-designed composites depend less on the resin matrix to transfer stress between fibres, so the effect of low matrix fraction of the SACFRP is less pronounced for the layup-designed laminates than their UD counterparts.

Table 5 lists specific tensile strength, modulus and toughness of the layup-designed CFRP and SACFRP.

3.5. LVI performance of layup-designed SACFRPs

Fig. 16 (a), (b), and (c) depict the curves of force-time, force-

Table 5
Specific tensile strength, modulus and toughness of the layup-designed CFRP and SACFRP.

Properties	CFRP	SACFRP
Specific tensile strength (MPa·cm^3/g)	411.72 ± 11.15	346.72 ± 8.71
Specific tensile modulus (GPa·cm^3/g)	29.44 ± 0.68	27.60 ± 1.00
Specific tensile toughness (MPa·cm^3/g)	3.81 ± 0.40	3.38 ± 0.58

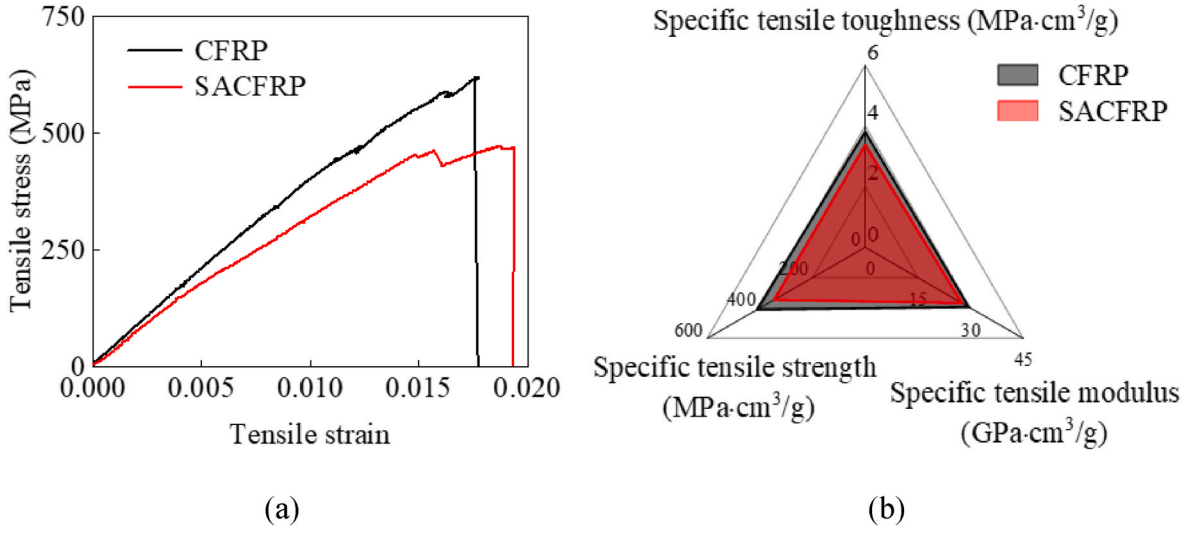

Fig. 15. (a) Tensile stress-strain curves, and (b) comparison between specific tensile modulus, strength, and toughness of the CFRP and SACFRP specimens with the stacking sequence of $[45/90/135/0]_s$.

displacement, and energy-time, respectively, of the lay-up designed CFRP and SACFRP specimens during 25J LVI tests. As illustrated in Fig. 16(a) and (b), the force-time and force-displacement responses exhibit more significant oscillations for the CFRP references than those for the SACFRP laminates, indicating that more severe damage occurred in the CFRP. Besides, the considerable drop after the peak value demonstrates drastic damage in CFRP laminates, as shown in Fig. 16 (a). On the other hand, for the SACFRP laminates, the initial force drop indicated the onset of damage, followed by a further and slight increment of force until reaching the next peak value. The highly smooth force-time and force-displacement responses imply minimal damage in the SACFRP laminates. Moreover, the plateau-shaped energy-time curves in Fig. 16 (c) suggest no perforation in the lay-up designed SACFRP and CFRP specimens. Therefore, the impact-resistant performance of SACFRP was effectively enhanced via the lay-up design, in contrast to the LVI test results of the UD specimens in section 3.3.

Fig. 17 presents a radar plot based on the impact characteristics of the layup-designed SACFRP and CFRP during 25J LVI tests. In this work, structural integrity is defined as the reciprocal value of the integrity loss. Despite the lower stiffness, peak force, and elastic energy of the layup-designed SACFRP, its structural integrity loss is only 0.323 mm, which is much lower than the integrity loss of 1.585 mm for the CFRP reference. Thus, the layup-designed SACFRP laminates demonstrate superior impact-resistant performance, indicating that the modification of stacking sequences can leverage the effects of STG on SACFRPs.

As depicted in Fig. 18, analysis of high-speed camera results revealed distinct impact-resistant mechanisms between SACFRP and CFRP. Similar to other conventional thermoset or thermoplastic composites [9, 42], local damage was also observed in the CFRP during the LVI test, suggesting that the CFRP absorbed the impact energy through its internal local fracture. In contrast, DIC analysis based on the high-speed

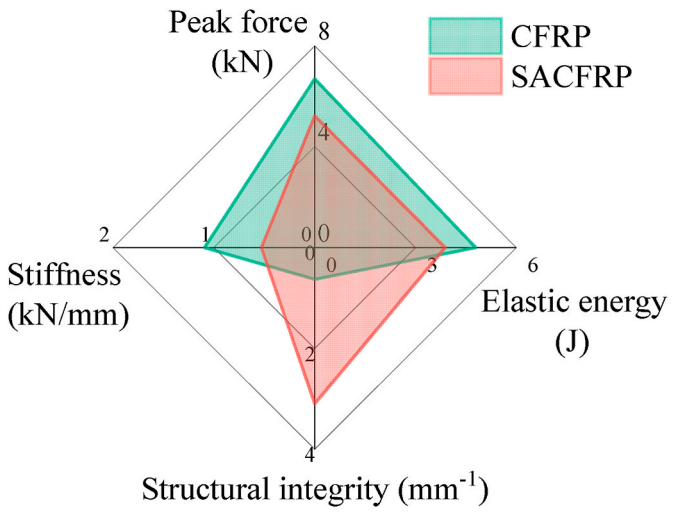

Fig. 17. Impact characteristics comparison of the layup-designed SACFRP and its CFRP reference during 25J LVI tests.

camera results found that the SACFRP experienced a unique impact-resistant process through its bending and rebounding behaviour, demonstrating that its energy absorption can be attributed to the global flexural behaviour of the laminated composite. Consequently, the SACFRP could maintain high structural integrity despite minor cracking resulting from the fixture that corresponds to the initial force drop illustrated in Fig. 16(a) and (b). Given that the impact mechanism transitions from local damage of CFRP to global bending of SACFRP, the newly developed composites demonstrate significant application

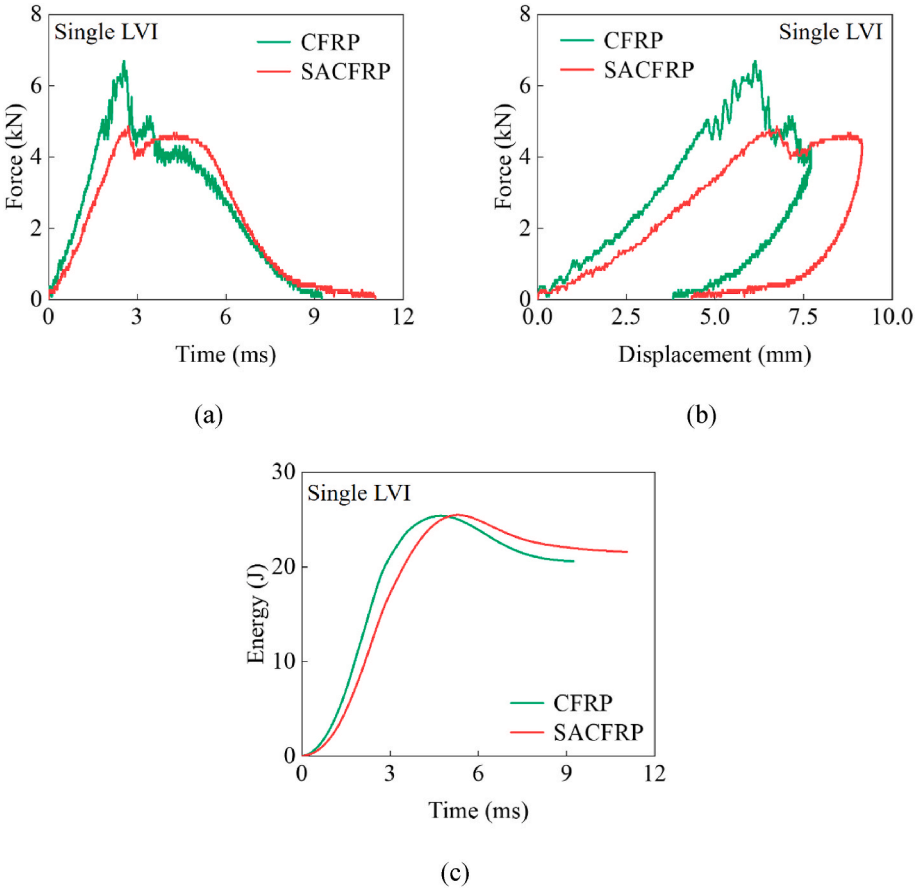

Fig. 16. (a) force-time, (b) force-displacement, and (c) energy-time responses of the layup-designed SACFRP and its CFRP reference during 25J LVI tests.

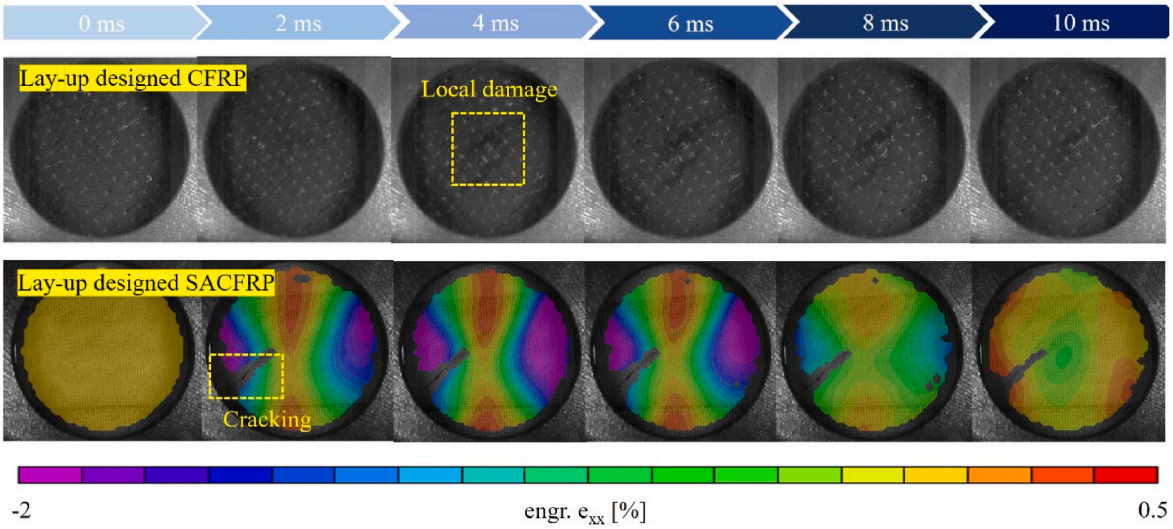

Fig. 18. Impact process of the lay-up designed CFRP and SACFRP under 25J LVI.

potential in engineering scenarios with complex unavoidable LVI. As can be found in section 3.8, the resistant mechanism of the SACFRP can be treated as purely elastic flexure and captured by Timoshenko's theoretical model. For further explanation, viscoelastic deformation and shear thickening behaviour of the STG can increase energy dissipation and enlarge the impact area [18,43]. Therefore, deformation can be distributed to the larger area of elastic fibres and matrix in the SACFRP under LVI, while the local damage is noted for the central impact region of the CFRP counterpart.

3.6. Recurring LVI (RLVI) performance of layup-designed SACFRPs

We conducted RLVI tests on the same position of specimens. Fig. 19 (a), (b), and (c) illustrate the force-time, force-displacement, and energy-time responses of the layup designed CFRP and SACFRP during RLVI tests. In the second 25J LVI test, the force rapidly diminishes to a very low level for the CFRP, suggesting the perforation, as depicted in Fig. 19 (a). In contrast, layup-designed SACFRPs demonstrated the ability to withstand 20 RLVIs without perforation, evidenced by the smoothly developed force-time and force-displacement behaviour of the SACFRP laminates during the twentieth LVI test, as demonstrated in

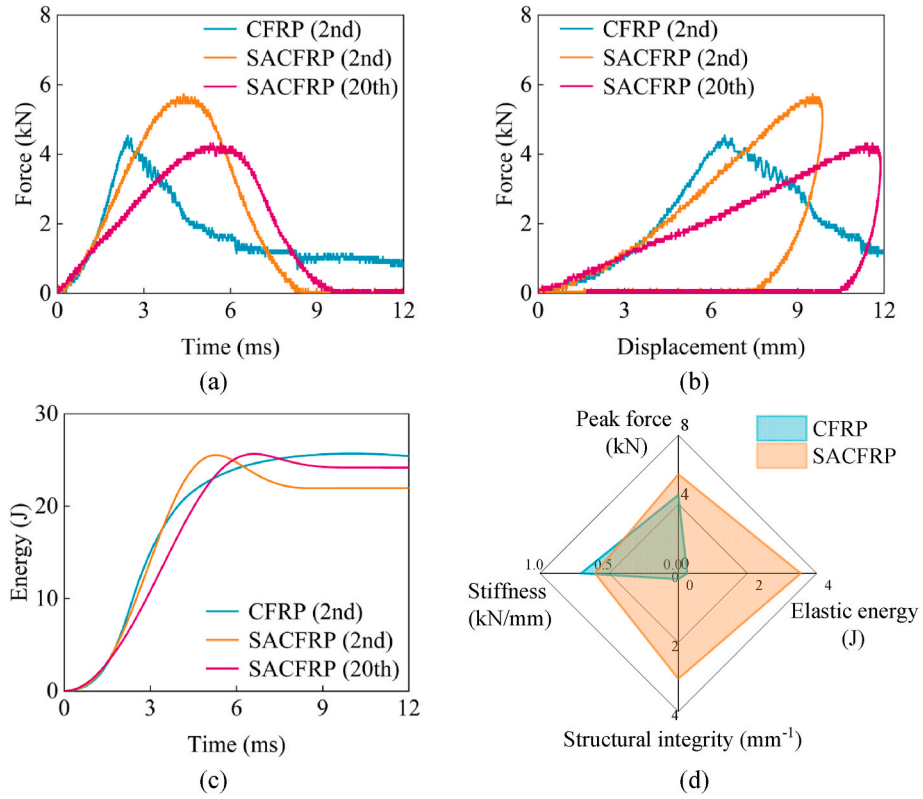

Fig. 19. (a) Force-time, (b) force-displacement, (c) energy-time responses and (d) impact characteristics comparison of lay-up designed SACFRP and its CFRP reference under recurring 25J LVI.

Fig. 19(a) and (b). There exists a force drop for layup-designed SACFRP, which can be attributed to the edge crack, as shown in Figs. 18 and 22 (d), due to the flexural behaviour under the first 25J LVI. The pre-existing edge crack provides more space for flexure of the layup-designed SACFRP under the second 25J LVI. Thus, there is no initial force drop, and the peak force can be higher for the second impact of the SACFRP. Fig. 19 (c) illustrates the plateau-shaped energy-time response of the SACFRP specimen under the 20th LVI, indicating good RLVI resistance of the developed composite laminates and no perforation occurrence. Fig. 19 (d) depicts the impact characteristics of the layup designed CFRP and SACFRP specimens under the second 25J LVI. The integrity loss of SACFRP is 0.328 mm under the second impact, which is much lower than the 5.922 mm integrity loss of the CFRP reference. Thus, SACFRPs demonstrate substantially improved impact-resistant performance under the RLVI condition.

Fig. 20 demonstrates impact process of the lay-up designed CFRP and SACFRP under the 25J RLVI. As shown in Fig. 20, the CFRP laminates experienced perforation during the second LVI, and the perforation occurred in the local damage area resulting from the initial impact. On the other hand, DIC analysis in Fig. 20 found that the flexural behaviour of the SACFRP laminate persisted during the RLVI despite that its rebounding performance was weakened progressively from the second to the twentieth impact. The less obvious rebounding behaviour aligned with the reduced elastic energy of the SACFRP during the 20th LVI test, as depicted in Fig. 19 (c). Although the maximum displacement increased with each impact, SACFRP could withstand the impact loads without perforation, indicating its highly enhanced toughness during RLVI tests. It can be inferred that the layup-designed SACFRP laminates exhibited significantly enhanced accumulated energy absorption. The incorporation of the STG as the interfacial enhancement material between carbon fibres and epoxy matrix improved the interfacial adhesion and toughness of the SACFRP, as also elaborated in section 3.2, leading to its superior impact-resistant performance under RLVI. Composite structures can be subjected to complex impact loads, such as repeated impacts, in real-world applications [44]. Hence, the remarkable impact resistance of the SACFRP under RLVI demonstrates its promising potential for diverse industrial utilisation.

Fig. 21 illustrates the variation of the impact characteristics for the layup-designed SACFRP under 25J RLVI. In Fig. 21 (a), the peak force increases during the 2nd and 3rd impact since the fibres bear more loads in the composite laminate, while the peak force drops sharply after the 3rd impact due to the fibre breakage [44]. The continuous decrease of the peak force corresponds to the progressive stiffness degradation. Particularly, the stiffness of SACFRP decreases obviously in Fig. 21 (b) due to accumulated integrity loss in the laminates after the 1st impact. Integrity loss of the SACFRP varies in the range from 0.5 mm to 1.0 mm for each impact in Fig. 21 (c). The stable development of integrity loss indicates high toughness of the layup-designed SACFRP laminates under RLVI. Fig. 21 (d) demonstrates that the elastic energy decreases initially and remains constant after the 5th impact. The initial decrease in the elastic energy corresponds to the fibre breakage and matrix damage that results in the significant stiffness drop. The following constant elastic energy indicates that SACFRP stably absorbs the impact energy through the flexural behaviour enabled by the STG during RLVI tests.

3.7. *The reliability of the impact-resistant performance of layup-designed SACFRP laminates during LVI tests*

This work specifically added repeatability of the impact performance of three layup-designed SACFRP specimens under 45J LVI, as this is the impact energy that clearly demonstrates the advantage of this newly designed material over the conventional CFRPs. For the other specimens, only one experiment was conducted for each of them due to time limitation. Still, the results under LVI with various impact energy values can reliably demonstrate the higher impact-resistant performance of SACFRP specimens compared to the CFRP counterparts. Fig. 22(a)–(c) illustrates the impact response of these specimens (S45J-1, S45J-2, and S45J-3) and the CFRP counterpart (C45J) during 45J LVI tests. The

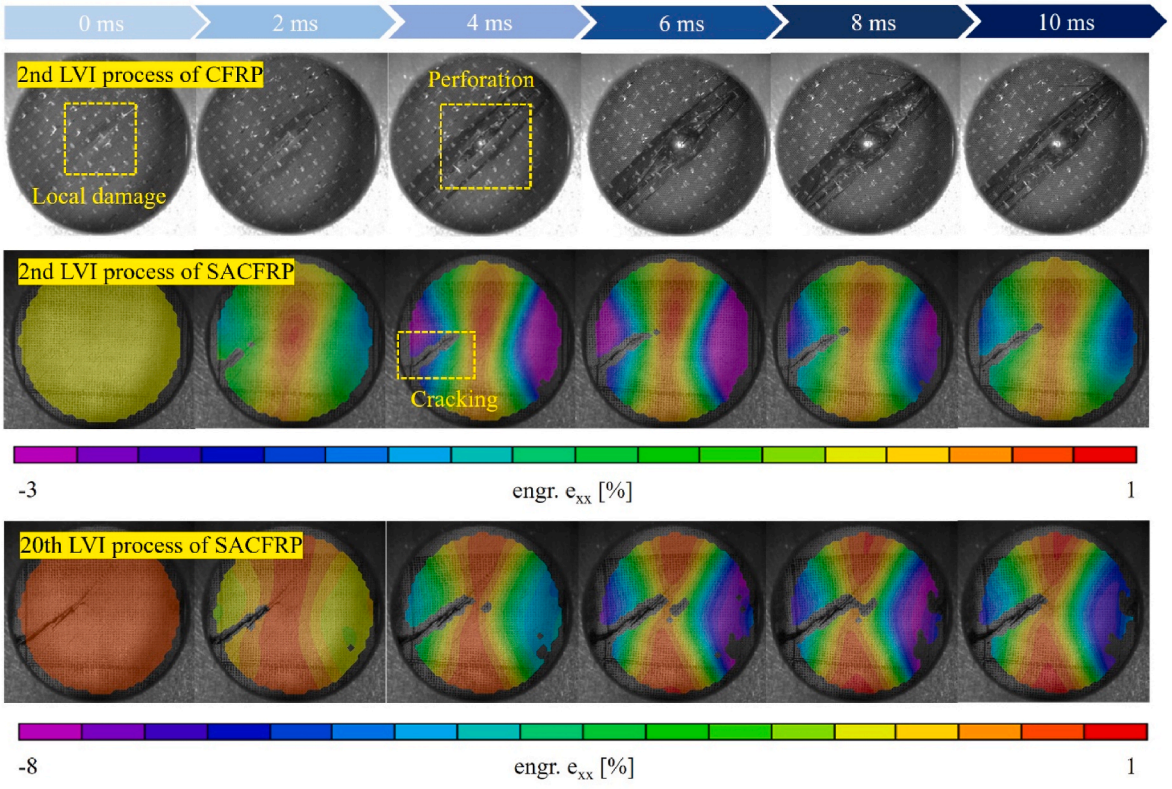

Fig. 20. Impact process of the layup-designed CFRP and SACFRP under the 25J RLVI.

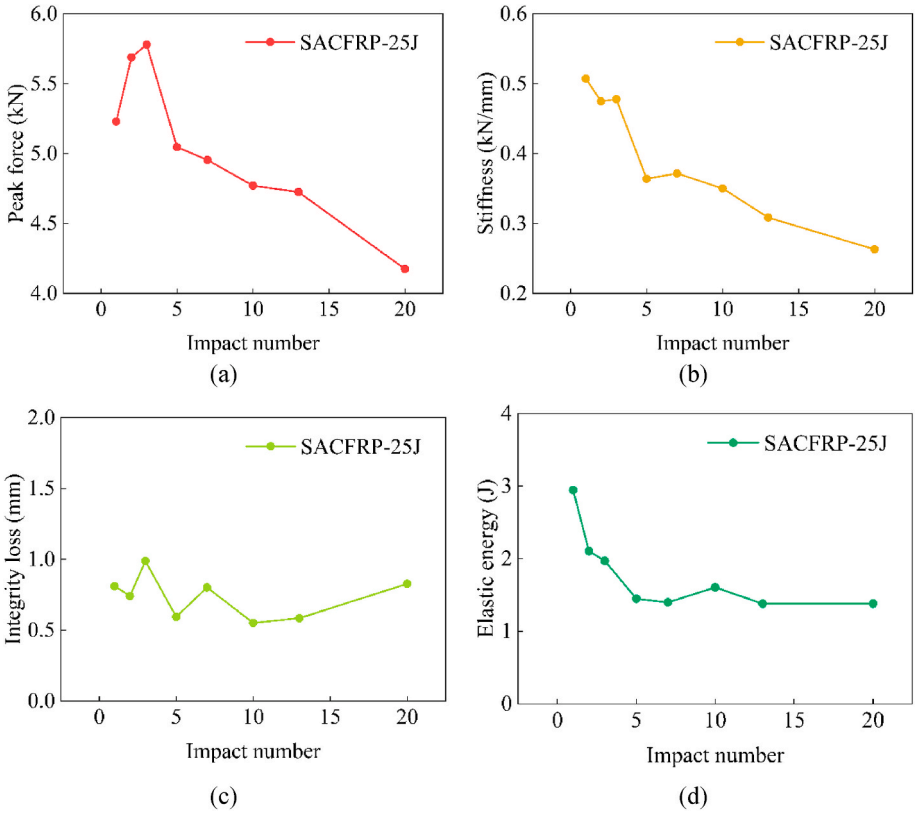

Fig. 21. The variations of (a) peak force, (b) stiffness, (c) integrity loss, and (d) elastic energy for the SACFRP under 25J RLVI.

highly smoother force-time responses indicate much less damage in SACFRP laminates compared to the sudden drop and large oscillation in the CFRP counterpart after the peak force, as demonstrated in Fig. 22 (a). Besides, a decrease in absorbed energy of the layup-designed SACFRP specimens corresponds to their rebounding behaviour during 45J LVI, while no decrease is noted for the CFRP counterpart, indicating the perforation. Moreover, the same stiffness illustrated in Fig. 22 (c) can reflect highly repeatable and stable impact performance of the layup-designed SACFRP laminates.

Fig. 22 (d) compares non-impact back surfaces of the SACFRP and CFRP specimens after 45J LVI. Severe local damage in the middle impact area can be observed for the CFRP specimen, exhibiting its brittleness under LVI conditions. By contrast, no obvious damage can be found in the middle impact area for the SACFRP specimen, demonstrating the high impact resistance and mechanism transition as discussed in section 3.5. The modelling-based validation is discussed in section 3.8 for the mechanism transition of the layup-designed SACFRP laminates. Besides, the crack developing from the edge in the S45J specimen corresponds to the initial force drop in Fig. 22 (a) and (c), resulting from the large flexure of layup-designed SACFRP laminates during LVI tests. Specifically, the sample edge of SACFRP laminates has a large rotation angle during LVI tests, requiring the occurrence of a crack on the edge to finish the whole flexural process.

Fig. 23 compares the effects of stacking sequence on the impact responses of the SACFRP under 35J LVI. As illustrated in Fig. 23 (a), the higher slope and peak force in the SACFRP laminate with the stacking sequence of $[45/90/135/0]_s$ indicate its higher impact-resistant performance compared to the SACFRP with the stacking sequence of $[0/90]_{2s}$. Besides, the shape of energy-time curves in Fig. 23 (b) demonstrated that both layup-designed SACFRP can resist 35J LVI, while the UD counterpart perforates under 25J LVI. Therefore, modifying the stacking sequence of SACFRP laminates can leverage the enhanced effect of the STG on the impact-resistant performance of its composite laminates. Future work will focus on the optimisation of the stacking sequence for SACFRP laminates.

Table 6 lists impact characteristics of the layup-designed ($[45/90/135/0]_s$) SACFRP (S) and CFRP (C) specimens under LVI with different impact energy values.

For further demonstration of impact-resistance of the newly developed lay-up designed SACFRP, its performance was also compared with the ultra-high molecular weight polyethylene (UHMWPE) composites. Among different types of fibres, the UHMWPE ones demonstrate much higher energy absorption. Particularly, energy absorption of the UHMWPE is typically 1.8, 2.6, and 33 times higher than that of carbon, aramid, and glass fibres, respectively [17,45]. Fig. 24 illustrates the comparison result for integrity loss of the SACFRP, UHMWPE fibre-reinforced thermoset polymer (PEFRP-S) and thermoplastic polymer (PEFRP-P) under LVI. It can be noted that the SACFRP exhibits significantly lower integrity loss than the PEFRP-S and PEFRP-P do [9]. Besides, quite limited increment is noticed for integrity loss of the SACFRP as the impact energy increases compared to the two PEFRP composites. Therefore, it can be concluded that the SACFRP demonstrates higher impact-resistant performance than the other typical FRPs.

3.8. Timoshenko's theoretical analysis for thin-plate flexure of the layup-designed SACFRP during LVI test

The DIC analysis shown in Fig. 18 demonstrates the impact-resistant mechanism transition under LVI conditions from brittle damage of the CFRP to flexure behaviour of the SACFRP. For simple theoretical analysis, the flexure process of the layup-designed SACFRP laminates is treated as a simply supported thin plate with a central concentrated force. Based on Timoshenko's analytical formula [46], the maximum deflection can be determined by using the following equation:

$$\omega_{\max} = \alpha \frac{Pa^2}{D} \tag{1}$$

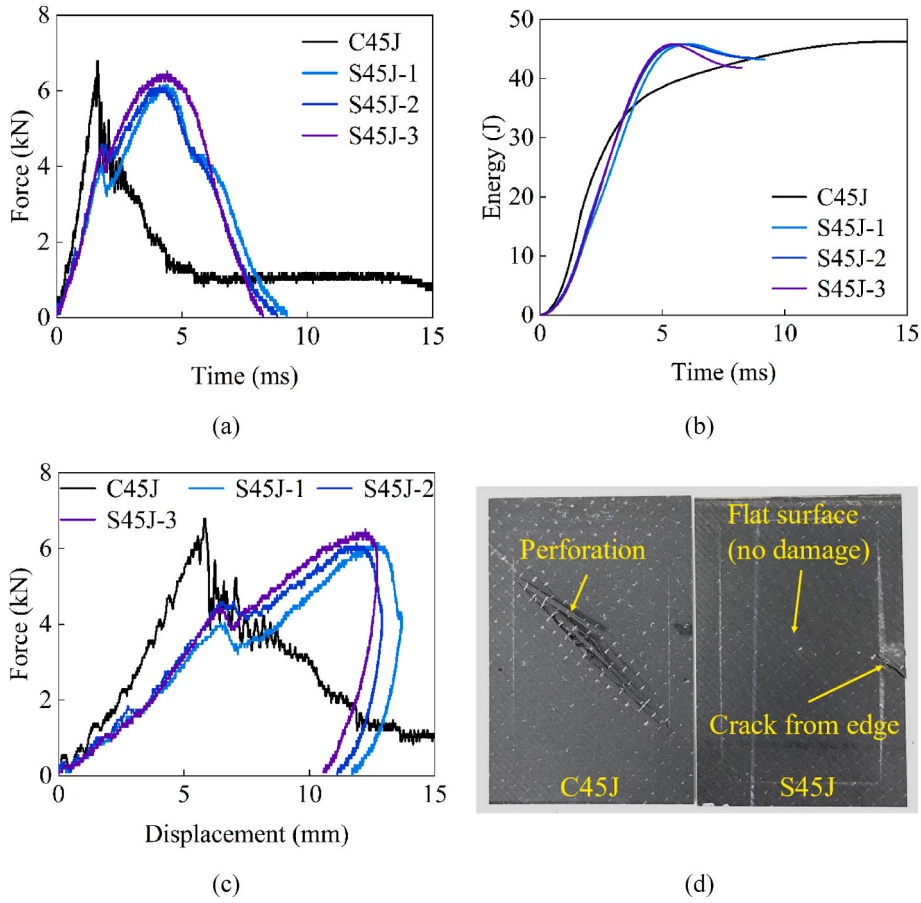

Fig. 22. (a) Force-time, (b) energy-time, and (c) force-displacement responses of three layup-designed SACFRP specimens (S45J-1, S45J-2, and S45J-3) and the corresponding CFRP counterpart (C45J) during 45J LVI tests, and (d) the comparison between non-impact back surfaces of the SACFRP and CFRP specimens after 45J LVI.

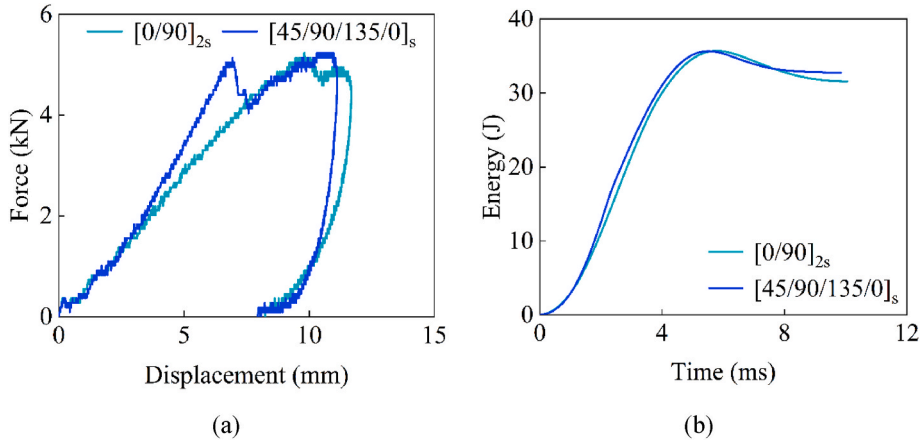

Fig. 23. (a) Force-displacement, and (b) energy-time responses of the SACFRP laminates with the stacking sequences of $[0/90]_{2s}$ and $[45/90/135/0]_s$.

where a represents the width of the thin plate, and P refers to the concentrated force applied on the centre of the thin plate. α is a numerical factor depending on the length-to-width ratio of specimens, which is 0.01527 here based on reference [46]. D can be calculated by using the following equation:

$$D = \frac{Eh^3}{12(1\text{-}\upsilon^2)} \tag{2}$$

in which E denotes Young's modulus, and it is the measured tensile modulus of the layup-designed SACFRP laminates in this work. υ refers to Poisson's ratio of the thin plate, and h denotes the specimen thickness. The concentrated force, P, can be determined using the following equation based on conservation of momentum for the impactor during LVI tests:

$$P = \mathrm{m}g + \frac{\mathrm{m}\Delta v}{\Delta t} \tag{3}$$

where m represents mass of the impactor, and g refers to the gravita-

Table 6
Impact characteristics of the layup-designed ($[45/90/135/0]_s$) SACFRP (S) and CFRP (C) specimens under LVI with different impact energies.

Impact characteristics	C25J	C45J	S25J	S35J	S45J
Fp (kN)	6.71	6.78	4.65	5.24	6.21 ± 0.17
PDm (mm)	6.13	5.83	8.82	10.67	12.39 ± 0.26
Fp/PDm (kN/mm)	1.09	1.16	0.53	0.49	0.50 ± 0.02
PDu (mm)	7.73	19.98	9.17	11.12	13.09 ± 0.39
PDu-PDm (mm)	1.60	14.15	0.35	0.45	0.69 ± 0.17
Ea (J)	20.65	45.23	21.66	32.82	42.95 ± 0.69
Ee (J)	4.65	0.00	3.64	3.02	2.83 ± 0.69

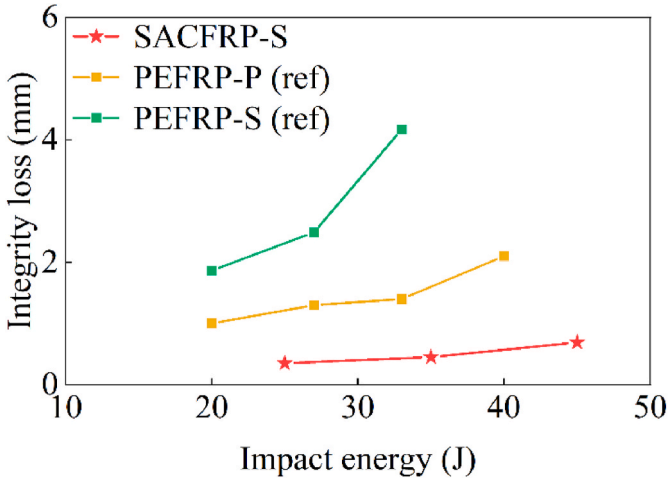

Fig. 24. Comparison of integrity loss between the SACFRP (SACFRP-S) in this work, the PEFRP-P and PEFRP-S [9] under LVI with various impact energy values.

tional acceleration. Δv refers to the impact velocity that can be calculated based on the impact energy. Δt is the impact time corresponding to the maximum absorbed impact energy. Table 7 provides parameters for Timoshenko's analytical model. h and Δt are averaged for layup-designed SACFRP laminates under 25J, 35J and 45J LVI.

Fig. 25 demonstrates a comparison between Timoshenko's analytical model and LVI test results for the maximum deflection of the layup-designed SACFRPs during LVI tests with various impact energies. The mean absolute percent error (MAPE) is merely 1.36 %. Therefore, the SACFRP laminates under LVI can be simply treated as elastic, instead of the brittle-fracture for conventional CFRP laminates, and the flexure behaviour can be accurately captured by Timoshenko's theoretical model.

4. Conclusion

This work incorporated STG into the CFRP composite laminates as the interphase material between the fibre reinforcement and the epoxy polymer matrix. The effects of the STG and layup design on the static and dynamic mechanical behaviour of the newly developed SACFRP were investigated. Specifically:

Table 7
Parameters for the Timoshenko's model to theoretically analyse flexural behaviour of the layup-designed SACFRP laminates during LVI tests.

Parameters	a (mm)	E (GPa)	υ	Averaged h (mm)	Averaged Δt (ms)
Layup-designed SACFRP	100	36.9	0.3	2.52	5.4

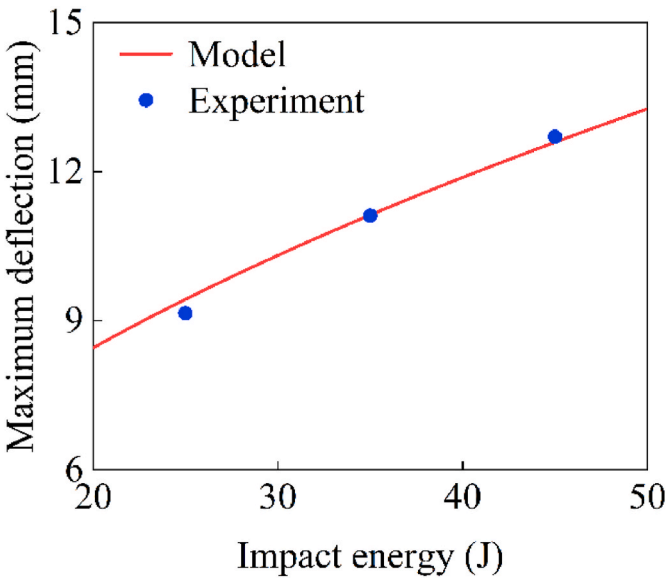

Fig. 25. Timoshenko's theoretical model to capture the flexure of the layup-designed SACFRP laminates under LVI as purely elastic.

1. Transverse tensile toughness of the UD SACFRP laminates increased by 138.95 % compared to CFRP references, demonstrating their substantial increase in the interfacial toughness. The SEM-based analysis further verified the enhanced interfacial adhesion of SACFRP compared with its CFRP reference.
2. The reduced epoxy matrix limits stress transfer and interlaminar properties of the UD SACFRP laminates under static mechanical loading. Proper layup design of the SACFRP laminates can alleviate the influence of the reduced matrix by redistributing most of the loading to the fibres along different orientations. As a result, the specific tensile toughness, modulus, and strength retentions of the layup-designed SACFRP laminates can achieve 88.8 %, 93.7 %, and 84.2 %, respectively, of the corresponding properties of the CFRP reference.
3. The structural integrity loss of the layup-designed SACFRP laminates decreased by 79.63 % compared to the CFRP references, indicating their enhanced impact-resistant performance. DIC analysis revealed that the SACFRP underwent the bending and rebounding process during LVI, suggesting that its energy absorption is primarily attributed to flexural behaviour. In contrast, the LVI tests on the CFRP highlighted its localised damage, indicating that the internal fracture mechanism predominantly drove its energy absorption.
4. Compared to perforation of the layup-designed CFRP at its second LVI, the layup-designed SACFRP could withstand the 20 RLVI events without perforation, indicating its higher accumulated impact energy absorption. The highly improved RLVI performance can be attributed to the enhanced interfacial adhesion and toughness of the SACFRP.
5. Further study will focus on the numerical modelling for impact behaviour of the STG and SACFRP, assisting optimisation of the STG fraction and the stacking sequence of SACFRP to balance the mechanical static properties and impact resistance. In addition, environmental effects on the performance of the SACFRP, such as hygrothermal ageing, UV exposure, or chemical resistance, will be investigated. Besides, fabrication techniques are supposed to be further improved for scaling up the manufacturing of the SACFRP.

CRediT authorship contribution statement

Wanrui Zhang: Writing – review & editing, Writing – original draft, Visualization, Methodology, Investigation, Formal analysis, Data

curation, Conceptualization. **Jianchao Zou:** Resources, Methodology, Investigation, Formal analysis, Conceptualization. **Zongyou Wei:** Investigation. **Zhibin Han:** Investigation. **Lei Yang:** Resources, Funding acquisition. **Weizhao Zhang:** Writing – review & editing, Supervision, Resources, Project administration, Funding acquisition.

Declaration of competing interest

The authors declare that they have no known competing financial interests or personal relationships that could have appeared to influence the work reported in this paper.

Acknowledgment

The work described in this paper was supported by grants from the Research Grants Council of the Hong Kong Special Administrative Region, China (Project No. CUHK 14205923), Innovation and Technology Commission of the Hong Kong Special Administrative Region, China (Project No. ITS/222/23), and the Natural Science Foundation of Shenzhen, China (Grant No. 20220809155933002).

Data availability

Data will be made available on request.

References

[1] L. Liu, et al., Effects of hygrothermal aging and re-drying on the translaminar fracture toughness of CFRP, Compos. Struct. (2025) 119137.
[2] D. Sun, et al., A coupled 3D hyper-viscoelastic constitutive model for thin woven composite prepregs in preforming and consolidation, Compos. B Eng. (2025) 112514.
[3] Z. Han, et al., Manufacturing carbon fabric composite structural batteries using spray with high-pressure and high-temperature and vacuum-bag assisted infusion techniques, Compos. Sci. Technol. 245 (2024) 110321.
[4] J. Zhang, et al., Past, present and future prospective of global carbon fibre composite developments and applications, Compos. B Eng. 250 (2023) 110463.
[5] M. Wang, et al., Effect of carbon/Kevlar asymmetric hybridization ratio on the low-velocity impact response of plain woven laminates, Compos. Struct. 276 (2021) 114574.
[6] L. Liu, et al., Experimental study of quasi-static and dynamic tensile behavior of epoxy resin under cyclic hygrothermal aging, Polym. Degrad. Stabil. 200 (2022) 109940.
[7] Z. Wang, Y. Li, Drop-weight impact and compressive properties of repeatable self-healing carbon fiber reinforced composites, Compos. B Eng. (2024) 111626.
[8] M. Russo, et al., Low velocity impact (LVI) simulation of a CFRP ply-drop laminates: a numerical analysis, in: International Symposium on Dynamic Response and Failure of Composite Materials, Springer, 2024.
[9] M.E. Kazemi, et al., Low-velocity impact behaviors of a fully thermoplastic composite laminate fabricated with an innovative acrylic resin, Compos. Struct. 250 (2020) 112604.
[10] E. Zhao, et al., Experimental study on multiple self-healing and impact properties of 2D carbon fiber fabric-reinforced epoxy composites with shape memory properties, Thin-Walled Struct. 205 (2024) 112549.
[11] A. Klingler, et al., Low velocity impact resistance of thin and toughened carbon fibre reinforced epoxy, Compos. Sci. Technol. 230 (2022) 109362.
[12] Z. Lei, et al., Low-velocity impact and compression-after-impact behaviors of twill woven carbon fiber/glass fiber hybrid composite laminates with flame retardant epoxy resin, Compos. Struct. 321 (2023) 117253.
[13] B. Sozen, et al., Comparison of the dynamic characteristics of GFRP, CFRP, and hybrid composites subjected to repeated low-velocity impact, Polym. Compos. (2024).
[14] K. Yang, et al., Integrating tough Antheraea pernyi silk and strong carbon fibres for impact-critical structural composites, Nat. Commun. 10 (1) (2019) 3786.
[15] L. Yang, et al., Experimental study on the impact resistance and damage tolerance of thermoplastic FMLs, Thin-Walled Struct. 196 (2024) 111435.
[16] A. Cengiz, İ.M. Yıldırım, E. Avcu, Flexural and low velocity impact behaviour of hybrid metal wire mesh/carbon-fibre reinforced epoxy laminates, Compos. Commun. 46 (2024) 101844.
[17] M.E. Kazemi, et al., A review on the hybrid titanium composite laminates (HTCLs) with focuses on surface treatments, fabrications, and mechanical properties, Compos. Appl. Sci. Manuf. 128 (2020) 105679.
[18] S. Zhang, et al., Study the safeguarding performance of shear thickening gel by the mechanoluminescence method, Compos. B Eng. 180 (2020) 107564.
[19] X. Zhang, et al., Mechanical response of shear thickening fluid filled composite subjected to different strain rates, Int. J. Mech. Sci. 196 (2021) 106304.
[20] F. Chen, et al., Gradient shear thickening gel/Kevlar fabric multi-layer armor with enhanced impact attenuation property, Compos. Struct. 330 (2024) 117829.
[21] Z. Xie, et al., Design of the ballistic performance of shear thickening fluid (STF) impregnated kevlar fabric via numerical simulation, Mater. Des. 226 (2023) 111599.
[22] P. Valizadeh, S.M. Hosseini, H. Alvandi, Studying the physical and mechanical behavior of fibre-reinforced epoxy composite, fabricated by VARTM and VB, in: The 3rd International Conference on Composites: Characterization, Fabrication and Application (CCFA-3), 2012.
[23] EPOLAM 5015 Datasheet, in: A. technology (Ed.), 2008. https://www.jacomp.fi/wp-content/uploads/2013/07/epolam5015-5014-5016.pdf.
[24] W. Zhang, et al., Experimental characterization and numerical prediction for mechanical aging of epoxy and its carbon fiber-reinforced composite under hydrothermal conditions, Polym. Compos. (2024).
[25] W.Z. Jianchao Zou, Weizhao Zhang, GEL ELASTOMER WITH SELF-HEALING AND HIGH-STRAIN-RATE RELATED PROPERTIES, US Provisional Patent Application No: 63/742,981, January 8, 2025.
[26] A. Standard, Standard Test Method for Tensile Properties of Polymer Matrix Composite Materials, American Society of Testing and Materials D, 2008, p. 3039.
[27] D. Astm, 'Standard test method for shear properties of composite materials by the V-notched beam method', 5379, Annu. Book ASTM (Am. Soc. Test. Mater.) Stand. 100 (1993) 235–247.
[28] A.C.D.o.C. Materials, Standard Test Method for Measuring the Damage Resistance of a fiber-reinforced Polymer Matrix Composite to a drop-weight Impact Event: D7136/D7136M-15, ASTM International, 2015.
[29] R.R. Rashapov, J. Unno, J.T. Gostick, Characterization of PEMFC gas diffusion layer porosity, J. Electrochem. Soc. 162 (6) (2015) F603.
[30] Q. He, et al., Impact resistance of shear thickening fluid/Kevlar composite treated with shear-stiffening gel, Compos. Appl. Sci. Manuf. 106 (2018) 82–90.
[31] A. Zhou, et al., Structural performance of FRP confined seawater concrete columns under chloride environment, Compos. Struct. 216 (2019) 12–19.
[32] A. Wongsto, S. Li, Micromechanical FE analysis of UD fibre-reinforced composites with fibres distributed at random over the transverse cross-section, Compos. Appl. Sci. Manuf. 36 (9) (2005) 1246–1266.
[33] H. Wang, et al., Micromechanical modeling for longitudinal tensile property of unidirectional CFRP considering dispersion of fiber properties, Compos. Struct. 339 (2024) 118081.
[34] Z. Lei, et al., Exploring the Iosipescu method to investigate interlaminar shear fatigue behavior and failure mechanisms of carbon fiber reinforced composites, Int. J. Fatig. 178 (2024) 108020.
[35] Z. Chen, et al., A comparative study of two astm shear test standards for chopped carbon fiber smc, SAE Int. J. Mater. Manuf. 11 (4) (2018) 277–284.
[36] L. Zubillaga, et al., An experimental study on matrix crack induced delamination in composite laminates, Compos. Struct. 127 (2015) 10–17.
[37] S.P. Shah, M. Maiarù, Effect of manufacturing on the transverse response of polymer matrix composites, Polymers 13 (15) (2021) 2491.
[38] X. Yuan, et al., Prediction of temperature-dependent transverse strength of carbon fiber reinforced polymer composites by a modified cohesive zone model, Compos. Struct. 304 (2023) 116310.
[39] W. Zhang, et al., Investigating the role of fibre-matrix interfacial degradation on the ageing process of carbon fibre-reinforced polymer under hydrothermal conditions, Compos. Sci. Technol. 259 (2025) 110922.
[40] A. Arteiro, et al., Micro-mechanical analysis of the effect of ply thickness on the transverse compressive strength of polymer composites, Compos. Appl. Sci. Manuf. 79 (2015) 127–137.
[41] K. Tangthana-umrung, M. Gresil, Interlaminar fracture toughness behaviour of carbon fibre reinforced polymer with epoxy-dicarboxylic acid vitrimer matrix, Compos. Commun. 32 (2022) 101182.
[42] M.E. Kazemi, et al., Investigating the roles of fiber, resin, and stacking sequence on the low-velocity impact response of novel hybrid thermoplastic composites, Compos. B Eng. 207 (2021) 108554.
[43] Y. Wang, et al., Dynamic behavior of magnetically responsive shear-stiffening gel under high strain rate, Compos. Sci. Technol. 127 (2016) 169–176.
[44] B. Liao, et al., Damage accumulation mechanism of composite laminates subjected to repeated low velocity impacts, Int. J. Mech. Sci. 182 (2020) 105783.
[45] M. Kazemi, et al., Mechanical properties and failure modes of hybrid fiber reinforced polymer composites with a novel liquid thermoplastic resin, elium®, Compos. Appl. Sci. Manuf. 125 (2019) 105523.
[46] S. Timoshenko, S. Woinowsky-Krieger, Theory of Plates and Shells, 2, McGraw-hill, New York, 1959.